Variations in atmospheric CO_2 growth rates coupled with tropical temperature

Weile Wang[a,b,1], Philippe Ciais[c], Ramakrishna R. Nemani[d], Josep G. Canadell[e], Shilong Piao[f,g], Stephen Sitch[h], Michael A. White[i], Hirofumi Hashimoto[a,b], Cristina Milesi[a,b], and Ranga B. Myneni[j]

[a]Division of Science and Environmental Policy, California State University Monterey Bay, Seaside, CA 93955; [b]Biospheric Science Branch, National Aeronautics and Space Administration Ames Research Center, Moffett Field, CA 94035; [c]Laboratoire des Sciences du Climat et de l'Environnement, 91191 Gif-sur-Yvette Cedex, France; [d]Advanced Supercomputing Division, National Aeronautics and Space Administration Ames Research Center, Moffett Field, CA 94035; [e]Global Carbon Project, Commonwealth Scientific and Industrial Research Organisation Marine and Atmospheric Research, Canberra, ACT 2601, Australia; [f]Department of Ecology, Peking University, Beijing 100871, China; [h]Department of Geography, University of Exeter, Exeter EX4 4RJ, United Kingdom; [g]Institute of Tibetan Plateau Research, Chinese Academy of Sciences, Beijing 100085, China; [i]Department of Watershed Sciences, Utah State University, Logan, UT 84322; and [j]Department of Earth and Environment, Boston University, Boston, MA 02215

Edited by Robert E. Dickinson, The University of Texas at Austin, Austin, TX, and approved June 26, 2013 (received for review November 13, 2012)

Previous studies have highlighted the occurrence and intensity of El Niño–Southern Oscillation as important drivers of the interannual variability of the atmospheric CO_2 growth rate, but the underlying biogeophysical mechanisms governing such connections remain unclear. Here we show a strong and persistent coupling ($r^2 \approx 0.50$) between interannual variations of the CO_2 growth rate and tropical land–surface air temperature during 1959 to 2011, with a 1 °C tropical temperature anomaly leading to a 3.5 ± 0.6 Petagrams of carbon per year (PgC/y) CO_2 growth-rate anomaly on average. Analysis of simulation results from Dynamic Global Vegetation Models suggests that this temperature–CO_2 coupling is contributed mainly by the additive responses of heterotrophic respiration (Rh) and net primary production (NPP) to temperature variations in tropical ecosystems. However, we find a weaker and less consistent ($r^2 \approx 0.25$) interannual coupling between CO_2 growth rate and tropical land precipitation than diagnosed from the Dynamic Global Vegetation Models, likely resulting from the subtractive responses of tropical Rh and NPP to precipitation anomalies that partly offset each other in the net ecosystem exchange (i.e., net ecosystem exchange ≈ Rh − NPP). Variations in other climate variables (e.g., large-scale cloudiness) and natural disturbances (e.g., volcanic eruptions) may induce transient reductions in the temperature–CO_2 coupling, but the relationship is robust during the past 50 y and shows full recovery within a few years after any such major variability event. Therefore, it provides an important diagnostic tool for improved understanding of the contemporary and future global carbon cycle.

climate–carbon cycle coupling | tropical land surface temperature | global dynamic vegetation model

Significant statistical relationships have been reported between interannual variations in the atmospheric CO_2 growth rate and global temperatures (1–4), precipitation (5), and El Niño–Southern Oscillation (ENSO) (2, 6–8). However, because the variability of the CO_2 growth rate is governed by many interacting processes of the coupled climate–carbon cycle system, interpreting the biogeophysical mechanisms underlying these statistical relationships remains a difficult task. For instance, studies on the lagged negative correlations ($r \approx -0.4$) between CO_2 growth rate and global temperature (3, 9) attributed such lagged couplings to delayed vegetation responses to temperature in the northern mid- to high (40° N to 60° N) latitudes, but studies on ENSO–CO_2 correlations ($|r| \approx 0.5$) (7, 10) suggested that these largely synchronous couplings are contributed from the responses of tropical ecosystems to concurrent climate variations. Early studies (2, 6) tended to focus on ENSO's impacts on oceanic carbon fluxes, whereas later analyses on isotope data (11, 12) and atmospheric inversion results (13–16) showed that terrestrial ecosystems have larger controls on CO_2 growth-rate variability. Process-based global terrestrial ecosystem models have been used to address this question (e.g., refs. 7, 17, 18). Driven with observed climate, several model simulations suggested that the interannual variability of CO_2 growth rate is mainly influenced by precipitation-regulated variations of tropical net ecosystem exchange (NEE) (7, 17). However, the sensitivity of modeled NEE to precipitation variations needs to be verified with independent observations (19, 20). After all, model simulated global NEE can only explain ~25% ($r^2 \approx 0.25$) of the interannual variance of CO_2 growth rate (7, 17), not significantly better than the explanation power of ENSO indices.

In this study, by using up-to-date atmospheric CO_2 and land-surface climate observations, we present rigorous correlation analysis in support of ENSO's direct (i.e., with response times of a few months) regulation on the CO_2 growth-rate variability via its impacts on tropical (24° S to 24° N) NEE (2, 7, 8). Importantly, this ENSO forcing appears to be exerted mainly through tropical temperature rather than precipitation. Our analysis also confirms previous findings (3, 9) that land surface temperatures in the tropics or other latitudes are negatively correlated with the CO_2 growth rate at response time lags of ~1.5 y. However, these delayed negative correlations are weaker than the direct positive coupling between tropical temperatures and the CO_2 growth rate, and are secondary in explaining the atmospheric CO_2 variability. Because correlations do not necessarily imply causality, we carefully examine the biogeophysical processes that plausibly underpin the identified coupling between tropical temperature and the atmospheric CO_2 growth rate.

Data and Methods

We compiled monthly atmospheric CO_2 concentration data between 1959 and 2011 from the National Oceanic and Atmospheric Administration Earth System Research Laboratory (ESRL) (2, 21, 22) and two sets of long-term climate data from three main sources, including global surface temperature (23) from National Aeronautics and Space Administration Goddard Institute for Space Studies, temperature and precipitation from the Climatic Research Unit–National Centers for Environmental Prediction (CRU-NCEP) climate dataset (18), and precipitation records from the Global Precipitation Climatology Project (24). Monthly CO_2 growth rate is first calculated as the first-order difference of atmospheric CO_2 concentrations between two

Author contributions: W.W., P.C., and R.R.N. designed research; W.W. performed research; W.W., H.H., and C.M. analyzed data; and W.W., P.C., R.R.N., J.G.C., S.P., S.S., M.A.W., H.H., C.M., and R.B.M. wrote the paper.

The authors declare no conflict of interest.

This article is a PNAS Direct Submission.

[1]To whom correspondence should be addressed. E-mail: weile.wang@nasa.gov.

This article contains supporting information online at www.pnas.org/lookup/suppl/doi:10.1073/pnas.1219683110/-/DCSupplemental.

successive months. The long-term (50-y) mean seasonal cycle is then removed from the data before a 12-mo moving sum is applied to the data series to convert the monthly values into annual CO_2 growth rates. The annual CO_2 growth rate data are smoothed by multimonth running averages, and their long-term trend is removed by using a simple linear regression. Because CO_2 growth rates calculated from the Mauna Loa data (1959–2011) and those of the global network (1980–2011) (22) are highly consistent over the common period of 1980 to 2011, we combined the two data sources into one time series following the approach in ref. 18. Monthly tropical temperature and precipitation time series are aggregated over vegetated land surface area between latitudes 24° N and 24° S based on a land-cover map (25). Similar to the processing of CO_2 data series, 12-mo running averages are used to aggregate the monthly climate anomalies to annual values. We detrended the temperature and precipitation anomalies by linear regressions with a multiyear moving window. Detrending the data by alternative approaches did not qualitatively change the results discussed in the paper. The detrended time series of CO_2 growth rate, tropical (24° S to 24° N) land-based temperature, and precipitation (reversed in sign for easier comparison) are shown in Fig. 1.

We obtained gridded global simulations of carbon fluxes from terrestrial biosphere models of the Dynamic Global Vegetation Model (DGVM) comparison project [http://dgvm.ceh.ac.uk (17); model runs are the same as published in ref. 18]. The dataset provides annual estimates of ecosystem component fluxes by four DGVMs for the period of 1901 to 2008 and a fifth one for 1958 to 2008. The same CRU-NCEP climate fields were used to drive the five DGVMs. We calculated detrended anomalies of the annual carbon fluxes following the methods described earlier. Other datasets used in this study include the Multivariate ENSO Index (MEI) (26) and the Global Fire Emissions Database Version 3 (available from 1997 onward) (27).

We conducted correlation analysis by using time series of CO_2 growth rate and climate anomalies following the standard procedures (28). Because there are serial correlations in the time series induced by the smoothing of the data, we test the statistical significance of the correlation coefficients by Monte Carlo experiments to ensure the rigor of the statistical analysis. We also verify the significance tests by subsampling monthly data to annual time steps to remove the serial correlations (29). Both methods render consistent test results in our analysis.

Results and Discussion

Fig. 2 shows the lagged correlations between the detrended CO_2 growth rate and tropical (24° S to 24° N) land-based climate variables. The strongest coupling ($r \approx 0.7$, $P < 0.0001$) is found between the CO_2 growth rate and the concurrent tropical land temperature (Fig. 2), the latter alone explaining ~50% (i.e., $r^2 \approx 0.50$) of the variance of the former. Regression analysis of the two variables further indicates that a 1 °C temperature anomaly leads to a CO_2 growth rate anomaly of 3.5 ± 0.6 PgC/y (Petagrams, or 10^{15} grams of carbon per year), with the SD (σ) of the temperature-related CO_2 growth rate variations being ~0.7 PgC/y (Fig. 1). In comparison, the correlations of the CO_2 growth rate with the MEI or with the (reversed) tropical precipitation anomalies peak at $r \sim 0.5$ with a time lag of ~6 mo (Fig. 2; positive lags here and throughout the manuscript indicate that climate variables lead CO_2). MEI or tropical precipitation explains only ~25% (i.e., $r^2 \approx 0.25$) of the variance of the CO_2 growth rate, matching half of the corresponding explanatory power of tropical temperature. The correlations of the CO_2 growth rate with MEI or tropical precipitation become statistically insignificant when the time lag further increases to 1 to 2 y, whereas those with temperature in the tropics or other latitudes change to significant negative values ($r \approx -0.4$; Fig. 2).

The positive coupling between the CO_2 growth rate and concurrent tropical land temperature was previously reported (4) and confirmed in this study. The negative correlations between the CO_2 growth rate and the lagged global temperatures were studied previously (3) and mainly attributed to delayed vegetation

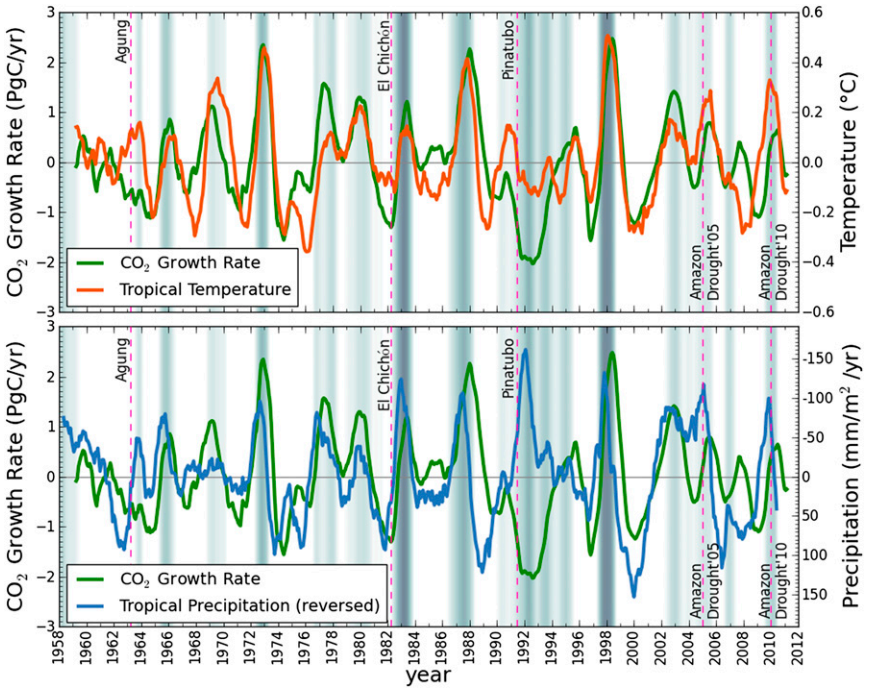

Fig. 1. Detrended anomalies of the atmospheric CO_2 growth rate, tropical (24°S to 24°N) land-surface air temperature, and tropical land precipitation. The precipitation anomalies are reversed in sign for easier comparison with the CO_2 growth rate and temperature. The background shading shows the occurrence and intensity of El Niño events as defined by the MEI.

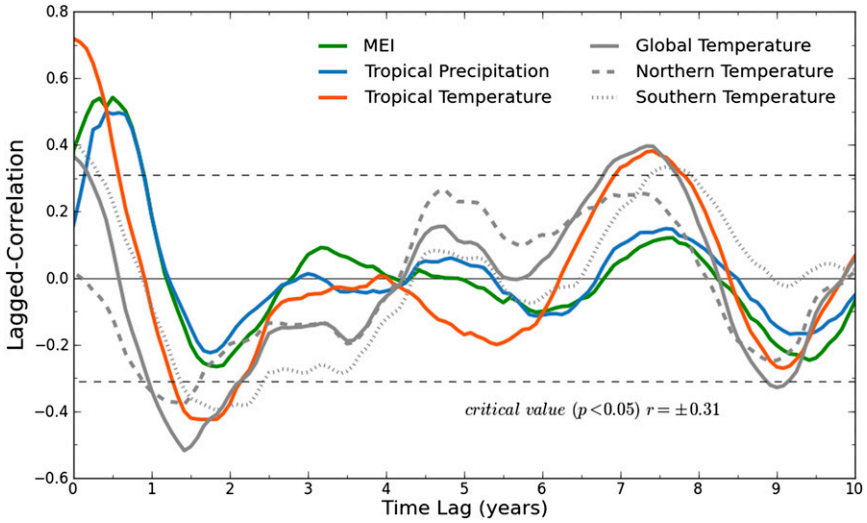

Fig. 2. Lagged correlations between interannual variations of the atmospheric CO_2 growth rate and tropical (24° S to 24° N) climate variables, including land surface temperature, land precipitation (reversed in sign), and the MEI. Positive time lags indicate that the climate variables lead the CO_2 growth rate. To facilitate comparisons with the findings of previous studies (3, 9), also shown here are the lagged correlations of CO_2 growth rate with land temperatures in northern latitudes (30° N to 70° N), southern latitudes (70° S to 30° S), and over the globe (90° S to 90° N). A time window of 42 y is applied to the time series so they have the same data length and the correlations have the same degrees of freedom. All the land-based climate variables are aggregated only over vegetated areas. The critical values for the correlations at 95% significance levels (i.e., $P < 0.05$) are estimated through two independent methods including Monte Carlo experiments with 10,000 samples (*Data and Methods*).

responses to temperature variations in the northern mid- to high latitudes (9). However, these lagged negative correlations are significantly weaker than the concurrent positive temperature–CO_2 coupling (Fig. 2) (4). Partial-correlation analysis also indicates that the lagged temperature (or MEI and tropical precipitation) anomalies are secondary to the concurrent tropical temperature in explaining the interannual variations of the CO_2 growth rate during the past 50 y (Fig. S1). In addition, whereas the lagged negative correlations seem to be contributed by temperatures in all latitudes (Fig. 2), the concurrent positive temperature–CO_2 coupling has a clear spatial predominance in the tropics (Fig. 2 and Fig. S2) and is directly associated with the influence of ENSO (as detailed later).

The fact that the CO_2 growth rate is more strongly coupled with tropical land temperature than with MEI or tropical land precipitation requires particular attention. Variations of tropical temperature and precipitation are usually driven by ENSO events and are therefore highly correlated with MEI as well as with each other ($|r| \approx 0.7$; Fig. 1). Because zonal shifts of tropical precipitation patterns respond more rapidly to ENSO developments than tropic-wide air temperature anomalies (30, 31), there is no apparent time lag between MEI and the land-based precipitation, and both lead temperature anomalies by ~5 mo (Fig. 1). Despite the time lags, the covarying relationships among these climate fields make it difficult to disentangle their individual influence on the atmospheric CO_2 growth rate (Fig. S3). However, these covarying relationships were lost during 1991 to 1994, when tropical temperature and precipitation anomalies were both much lower than would be expected from their normal couplings with ENSO and deviated from their usual negative correlation with each other (Fig. 1). These unusual climate anomalies were induced by the major volcanic eruption of Mount Pinatubo in June 1991, which injected large amounts of aerosols into the stratosphere to reduce incident solar energy (30, 32, 33). The period from 1991 to 1994 was also a period when MEI and tropical precipitation variations were decoupled from those of the CO_2 growth rate ($r = 0.0$–0.2; Fig. S3). During this period, the anomalies of tropical precipitation and the CO_2 growth rate varied in the opposite direction from their normal coupling (Fig. 1), complicating their explanation through the same relationship (as discussed later). In contrast, the corresponding temperature–CO_2 coupling, although weakened, remained within its normal level and statistically significant ($P < 0.05$; Fig. S3).

Global CO_2 fluxes from land-use changes and fossil fuel emissions have relatively small interannual variability ($\sigma = 0.1$–0.3 PgC/y) (18), accounting for 10% of the variance (σ^2) of the CO_2 growth rate ($\sigma = 1.0$ PgC/y; Fig. 1). Estimates of the interannual variability (σ) of global ocean CO_2 uptake are in the range of 0.2 to 0.5 PgC/y (14, 34, 35); however, ocean carbon processes operate to absorb, rather than release, extra CO_2 during El Niño years (35–37), which is different from the identified coupling between atmospheric CO_2 growth rate and MEI or the associated tropical climate anomalies. Emissions from wildfires can occasionally exceed 0.5 PgC/y during extreme years [e.g., the Indonesian peat-forest burning in 1997 and 1998 (38)], but their overall variability is low ($\sigma = 0.26$ PgC/y), at least during the period of the GFED dataset since 1997 (Fig. S4) (27). Therefore, it is generally believed that variations in global NEE—primarily the difference between heterotrophic respiration (Rh) and net primary production (NPP)—are mainly responsible for the interannual variability of the CO_2 growth rate (14, 18, 39). Satellite data-driven and ground observation-based estimates indicate that ~60% of global NPP and Rh are distributed in the tropics (40–43). Atmospheric inversion experiments (16, 44) and global vegetation model simulations (17, 18) also suggest that more than 60% of the interannual variance of global NEE originates from tropical land ecosystems (Fig. S5), consistent with the correlation analyses shown in Figs. 1 and 2.

However, the observation that tropical land temperature is a better predictor than precipitation in explaining tropical NEE (and the CO_2 growth rate) variability (Figs. 1 and 2) is not fully reproduced by the analyzed DGVM simulations (17). Rather, the interannual variability of tropical NEE in these models is dominated by the NPP component (Fig. S5 and Table S1), with the latter (i.e., NPP) being regulated mainly by tropical precipitation anomalies. The DGVM-simulated tropical NEE (and NPP) variations have a magnitude ($\sigma = 1.0$ PgC/y; Table S1)

directly comparable with the magnitude of the CO_2 growth rate (σ = 1.0 PgC/y; Fig. 1). However, the simulated tropical (and global) NEE anomalies are only moderately correlated with the CO_2 growth rate anomalies (r = 0.4–0.5; Table S2), explaining 25% ($r^2 \approx$ 0.25) of the variance of the latter. These discrepancies suggest that the analyzed DGVMs may have a common bias to overestimate the sensitivity of tropical NEE (and NPP) to precipitation.

To diagnose which bias in the DGVM formulations (or settings) produces their oversensitivity to precipitation would require detailed factorial simulations or response-function comparisons to idealized temperature and precipitation anomalies, which is beyond the scope of this study. Instead, we empirically determine a linear combination of the DGVM-simulated tropical NPP and Rh that best explains the observed variations of the CO_2 growth rate. We find that, by reducing the simulated tropical NPP variability to the magnitude of the simulated Rh variability (σ = 0.4–0.5 PgC/y; Table S1), we not only reduce the SD of the simulated tropical NEE anomalies to 0.7 PgC/y (Fig. 3) so that it is more consistent with the magnitude inferred from the coupling between tropical temperature and the CO_2 growth rate (Fig. 1), but also significantly improve the correlation (r) between the simulated NEE and the observed CO_2 growth rate from 0.5 to 0.7 (Fig. 3 and Table S2). The mechanism for this correlation improvement is illustrated in Fig. 3. Because tropical NPP and Rh are both positively regulated by precipitation (40, 45), their responses to precipitation variations are subtractive and partly offset each other in controlling tropical NEE anomalies. In contrast, tropical temperature regulates NPP and Rh in opposite directions [e.g., warmer anomalies in the tropics increase Rh and decrease NPP (4, 46, 47)], and such additive responses amplify the influence of tropical temperature on NEE (Fig. 3).

The finding that the analyzed DGVMs tend to overestimate the response of tropical NEE to precipitation variations questions their suitability for future carbon-cycle projections (48, 49). Some of the climatic events linked to such concerns are the severe droughts experienced by the Amazon basin in 2005 and 2010, which reportedly reduced tropical forest NPP by 1.6 to 2.2 PgC/y and increased tree mortality (50, 51). However, commensurate positive CO_2 growth-rate anomalies were not observed during 2005 or 2010—indeed, the responses of the CO_2 growth rate to the 2005 and the 2010 Amazon droughts were small compared with other ENSO-related droughts in the past 50 y (Fig. 1). Assuming that the large reductions of tropical NPP reported previously (50, 51) are realistic, the absence of marked variations of the global CO_2 growth rate after the 2005 and 2010 Amazon droughts may imply that the drought conditions also coincidently reduced tropical Rh along with NPP, resulting in (relatively) small NEE anomalies.

We further diagnose the impacts of climate extremes on the tropical carbon cycle by examining how the CO_2 growth rate deviates from the expected value predicted through a linear statistical model of CO_2 growth rate vs. tropical temperature anomalies. These deviations define a residual anomalous carbon flux (σ = 0.7 PgC/y, corresponding to the 50% unexplained interannual variance of the CO_2 growth rate; Fig. 4) that accounts

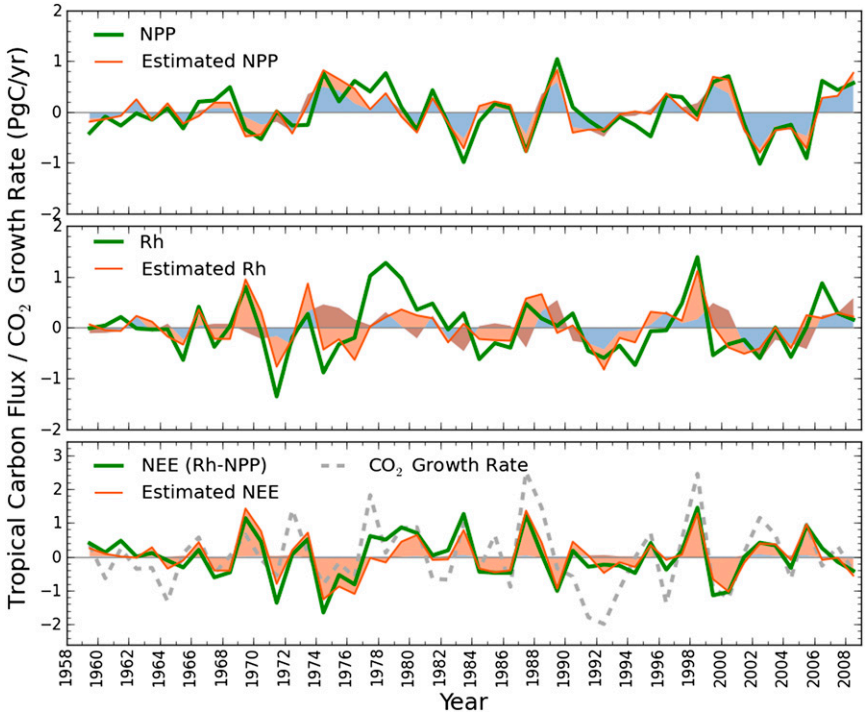

Fig. 3. Interannual variations in tropical terrestrial carbon fluxes (NPP, Rh, and NEE) simulated by four different previously described DGVMs (17, 18). The green lines represent the ensemble means of the DGVMs, with the magnitudes of the NPP and the Rh anomalies being optimized so the resulting NEE (Rh-NPP) best explains the variations of the observed atmospheric CO_2 growth rate (gray dashed line, *Bottom*; text and Tables S1 and S2]. The orange lines show the corresponding carbon fluxes estimated through linear regressions using concurrent tropical land-surface air temperature and land-based precipitation as the explanatory variables, which respectively capture 79%, 55%, and 83% of the variance of the model-simulated NPP, Rh, and NEE (green lines) by the r^2 statistics of the regression analyses. The orange and the blue shading, plotted as one stacking on another, indicate the individual contributions from temperature and precipitation to the estimated fluxes. As shown, tropical temperature and precipitation significantly ($P < 0.001$) contribute to the variability of NPP and Rh (*Top* and *Middle*). However, because precipitation positively regulates tropical NPP and Rh, its net effects on tropical NEE are weakened and statistically insignificant, such that the blue shading becomes indiscernible (*Lower*). In contrast, temperature regulates tropical NPP and Rh differently in sign so that its net effects on NEE (orange shading, *Bottom*) are strengthened.

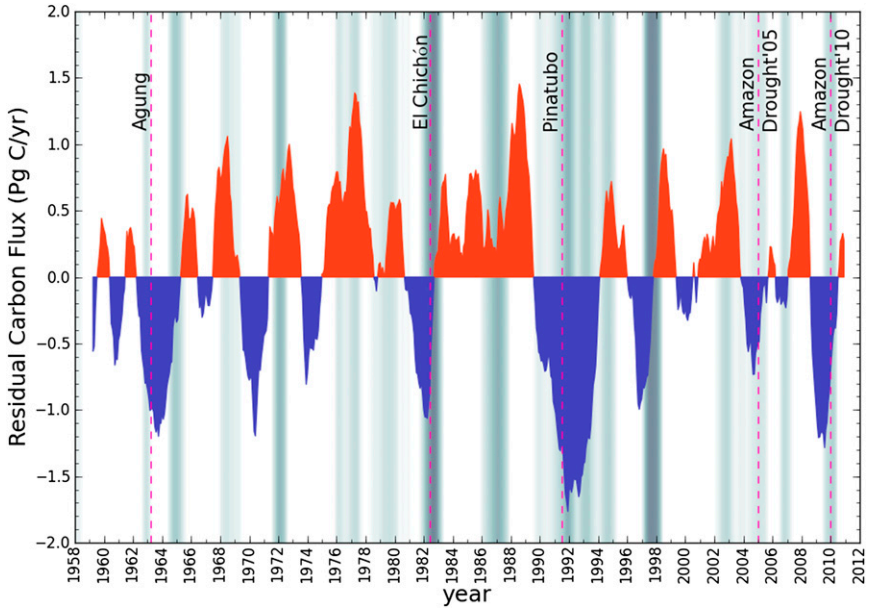

Fig. 4. Residual carbon flux anomalies estimated by the difference between the observed atmospheric CO_2 growth rate and those estimated from tropical land-surface temperature anomalies with a linear regression model. Positive values indicate carbon fluxes into the atmosphere (sources) and negative values indicate carbon fluxes into the surface (sinks). The background shading is the same as in Fig. 1. As shown, the extra carbon sink of 1990 to 1994 may have started 1 to 2 y before the eruptions of Mount Pinatubo. Therefore, it was most likely induced by multiple factors that concurred during that time (56) as detailed in the text.

for variations of NPP and Rh responding to climate drivers other than those represented by tropical temperature and variations in other carbon fluxes (e.g., fossil fuel emissions, wildfires variability). The estimated residual anomalies are robust in that they do not qualitatively change when either tropical land precipitation or MEI is included in the regression. For reasons discussed earlier, no significant residual-carbon-flux anomalies were observed following the 2005 Amazon drought in three consecutive years, or following the 2010 Amazon drought to the present (Fig. 4). A large positive anomaly (1.2 PgC/y) was seen after 2008, but it quickly switches to be negative in 2009 (−1.5 PgC/y; Fig. 4). The latter is too large to be explained by the 1.3% decrease (0.11 PgC/y) of fossil fuel emissions during the 2008 to 2009 global economic crisis (52), but most likely reflects the natural variability of the global carbon cycle induced by drivers other than tropical temperature or precipitation (as described later).

The most outstanding feature of Fig. 4 concerns the significant negative residual-carbon-flux anomalies (−1.7 PgC/y) during 1990 to 1994, which indicate an enhanced terrestrial carbon sink not explained by tropical land temperature and coincide with the decrease in the temperature's decadal correlations with the CO_2 growth rate (Fig. S3). Previous studies attributed these anomalies to reduced Rh (2, 33) and/or increased NPP in the northern hemisphere, the latter perhaps promoted by a transient increase in the diffuse fraction of solar radiation after the eruption of Mount Pinatubo in June 1991 (53–55). However, such mechanisms alone cannot fully explain the temporal evolution of the residual carbon flux anomalies, in which the switch to the extra sink started in mid-1989, approximately 2 y before the Pinatubo eruption (Fig. 4) and amid a period of greater than normal warmth (Fig. 1). We also do not see a similar extra carbon sink, but rather an extra source not explained by tropical temperature, in the residual carbon flux anomalies following the eruption of El Chichón in April 1982 (Fig. 4). Therefore, the extra carbon sink of 1990 to 1994 was most likely induced by multiple factors that concurred during that time (56). For instance, the shift of the residual carbon anomalies from an extra source in 1983 to 1989 to an extra sink in 1990 to 1994 may be more coherently explained by taking into account the increases in tropical (and global) NPP that were favored by the widespread declines in cloud cover over light-limited tropical rainforests in late-1980s and through 1990s (40, 57–59). Finally, we would like to point out that, if we calculate the residual carbon flux anomalies solely from the statistical coupling between the CO_2 growth rate and the tropical land-based precipitation, the estimated extra carbon sink for 1990 to 1994 will be significantly larger (3.1–3.8 PgC/y in absolute values; Fig. S6) than discussed earlier, and therefore more difficult to explain by the previously proposed biogeophysical mechanisms. This discrepancy imposes additional questions on the sensitivity of tropical ecosystems to precipitation variations at interannual time scales (19, 20, 49).

In summary, the strong and robust coupling between interannual variations of the atmospheric CO_2 growth rate and concurrent tropical temperature during the past 50 y provides a key diagnostic for our understanding of the global carbon cycle. This coupling cannot be justified by the delayed responses of mid- to high-latitude ecosystems to global temperature variations, nor may it be interpreted as an indirect reflection of the coupling between the CO_2 growth rate and tropical precipitation anomalies, which indeed is found to be weaker and less consistent. Instead, analyses of process-based global vegetation models indicate that this strong temperature–CO_2 coupling is best explained by the additive responses of tropical terrestrial respiration and primary production to temperature variations, which reinforce each other in enhancing temperature's control on tropical NEE. Although this explanation inherits the uncertainties associated with the current estimates of global carbon fluxes and needs to be further verified, we emphasize that the coupling itself, along with other observational constraints, must be reproduced by vegetation (or other related) models to realistically simulate the current status of the global carbon cycle and project its future changes.

ACKNOWLEDGMENTS. We thank all the researchers and their funding agencies who worked to provide the datasets for this study; C. Le Quéré, C. D. Jones, M. Reichstein, and three anonymous reviewers for constructive

comments on this manuscript; and F. Melton, S. Ganguly, G. Zhang, A. Michaelis, P. Votava, J. Xiong, and L. Xu for assistance in the analysis. This research was made possible using the NASA Earth Exchange (https://c3.nasa.gov/nex/), a "science as a service" collaborative for the geosciences community. NEX combines supercomputing, Earth system modeling, remote sensing data from NASA and other agencies, and a scientific social networking platform to deliver a complete work environment in which users can explore and analyze large Earth science data sets, run modeling codes, collaborate on new or existing projects, and share results within and/or among communities.

1. Kuo C, Lindberg C, Thomson DJ (1990) Coherence established between atmospheric carbon dioxide and global temperature. *Nature* 343(6260):709–714.
2. Keeling CD, Whorf TP, Wahlen M, van der Plicht J (1995) Interannual extremes in the rate of atmospheric carbon dioxide since 1980. *Nature* 375(6533):666–670.
3. Braswell BH, Schimel DS, Linder E, Moore B III (1997) The response of global terrestrial ecosystems to interannual temperature variability. *Science* 278(5339):870–873.
4. Adams JM, Piovesan G (2005) Long series relationships between global interannual CO2 increment and climate: evidence for stability and change in role of the tropical and boreal-temperate zones. *Chemosphere* 59(11):1595–1612.
5. Yang X, Wang M (2000) Monsoon ecosystems control on atmospheric CO_2 interannual variability: Inferred from a significant positive correlation between year-to-year changes in land precipitation and atmospheric CO_2 growth rate. *Geophys Res Lett* 27(11):1671–1674.
6. Bacastow RB (1976) Modulation of atmospheric carbon dioxide by the Southern Oscillation. *Nature* 261(5556):116–118.
7. Zeng N, Mariotti A, Wetzel P (2005) Terrestrial mechanisms of interannual CO_2 variability. *Global Biogeochem Cycles* 19(1), 10.1029/2004GB002273.
8. Raupach MR, Canadell JG, Le Quéré C (2008) Anthropogenic and biophysical contributions to increasing atmospheric CO2 growth rate and airborne fraction. *Biogeosciences* 5(6):1601–1613.
9. Vukićević T, Braswell BH, Schimel D (2001) A diagnostic study of temperature controls on global terrestrial carbon exchange. *Tellus B* 53(2):150–170.
10. Raddatz TJ, et al. (2007) Will the tropical land biosphere dominate the climate-carbon cycle feedback during the twenty first century? *Clim Dyn* 29(6):565–574.
11. Keeling CD, Revelle R (1985) Effects of El Niño/southern oscillation on the atmospheric content of carbon dioxide. *Meteoritics* 20(2):437–450.
12. Nakazawa T, Morimoto S, Aoki S, Tanaka M (1993) Time and space variations of the carbon isotopic ratio of tropospheric carbon-dioxide over Japan. *Tellus B* 45(3):258–274.
13. Ciais P, Tans PP, Trolier M, White JWC, Francey RJ (1995) A large northern hemisphere terrestrial CO_2 sink indicated by the $^{13}C/^{12}C$ ratio of atmospheric CO_2. *Science* 269(5227):1098–1102.
14. Bousquet P, et al. (2000) Regional changes in carbon dioxide fluxes of land and oceans since 1980. *Science* 290(5495):1342–1347.
15. Röedenbeck C, Houweling S, Gloor M, Heimann M (2003) CO_2 flux history 1982-2001 inferred from atmospheric data using global inversion of atmospheric transport. *Atmos Chem Phys* 3(6):1919–1964.
16. Baker DF, et al. (2006) TransCom 3 inversion intercomparison: impact of transport model errors on the interannual variability of regional CO_2 fluxes, 1988-2003. *Global Biogeochem Cycles* 20(1):GB1002, 10.1029/2004GB002439.
17. Sitch S, et al. (2008) Evaluation of the terrestrial carbon cycle, future plant geography and climate-carbon cycle feedbacks using five Dynamic Global Vegetation Models (DGVMs). *Glob Change Biol* 14(9):2015–2039.
18. Le Quéré C, et al. (2009) Trends in the sources and sinks of carbon dioxide. *Nat Geosci* 2(12):831–836.
19. Schwalm CR, et al. (2011) Does terrestrial drought explain global CO_2 flux anomalies induced by El Niño? *Biogeosciences* 8(9):2493–2506.
20. Ponce Campos GE, et al. (2013) Ecosystem resilience despite large-scale altered hydroclimatic conditions. *Nature* 494(7437):349–352.
21. Conway T, et al. (1994) Evidence of interannual variability of the carbon cycle from the NOAA/CMDL global air sampling network. *J Geophys Res* 99(D11):22831–22855.
22. Masarie KA, Tans PP (1995) Extension and integration of atmospheric carbon dioxide data into a globally consistent measurement record. *J Geophys Res* 100(D6):11593–11610.
23. Hansen J, Ruedy R, Glascoe J, Sato M (1999) GISS analysis of surface temperature change. *J Geophys Res* 104(D24):30997–31022.
24. Adler RF, et al. (2003) The version-2 Global Precipitation Climatology Project (GPCP) monthly precipitation analysis (1979-present). *J Hydrometeorol* 4(6):1147–1167.
25. Friedl MA, et al. (2002) Global land cover mapping from MODIS: Algorithms and early results. *Remote Sens Environ* 83(1):287–302.
26. Wolter K, Timlin MS (2011) El Niño/Southern Oscillation behaviour since 1871 as diagnosed in an extended multivariate ENSO index (MEI.ext). *Int J Climatol* 31(7):1074–1087.
27. van der Werf GR (2010) Global fire emissions and the contribution of deforestation, savanna, forest, agricultural, and peat fires (1997-2009). *Atmos Chem Phys* 10(23):11707–11735.
28. Enders W (1995) *Applied Econometric Time Series* (Wiley, New York).
29. Ebisuzaki W (1997) A method to estimate the statistical significance of a correlation when the data are serially correlated. *J Clim* 10(9):2147–2153.
30. Gu G, Adler RF (2011) Precipitation and temperature variations on the inter-annual time scale: Assessing the impact of ENSO and volcanic eruptions. *J Clim* 24(9):2258–2270.
31. Wallace JM, et al. (1998) On the structure and evolution of ENSO-related climate variability in the tropical pacific: Lessons from TOGA. *J Geophys Res* 103(C7):14241–14259.
32. Dutton EG, Bodhaine BA (2001) Solar irradiance anomalies caused by clear-sky transmission variations above Mauna Loa: 1958-99. *J Clim* 14(15):3255–3262.
33. Lucht W, et al. (2002) Climatic control of the high-latitude vegetation greening trend and Pinatubo effect. *Science* 296(5573):1687–1689.
34. Patra PK, et al. (2005) Interannual and decadal changes in the sea-air CO_2 flux from atmospheric CO_2 inverse modeling. *Global Biogeochem Cycles* 19(4):GB4013, 10.1029/2004GB002257.
35. Park G-H, Lee K, Wanninkhof R, Feely RA (2006) Empirical temperature-based estimates of variability in the oceanic uptake of CO_2 over the past 2 decades. *J Geophys Res* 111(C7), 10.1029/2005/JC003090.
36. Feely RA, et al. (2002) Seasonal and interannual variability of CO_2 in the equatorial Pacific. *Deep Sea Res Part II Top Stud Oceanogr* 49(13):2443–2469.
37. McKinley GA, Follows MJ, Marshall J (2004) Mechanisms of air-sea CO_2 flux variability in the equatorial Pacific and the North Atlantic. *Global Biogeochem Cycles* 18(2):GB2011, 10.1029/2003GB002179.
38. Page SE, et al. (2002) The amount of carbon released from peat and forest fires in Indonesia during 1997. *Nature* 420(6911):61–65.
39. Canadell JG, et al. (2007) Contributions to accelerating atmospheric CO_2 growth from economic activity, carbon intensity, and efficiency of natural sinks. *Proc Natl Acad Sci USA* 104(47):18866–18870.
40. Nemani RR, et al. (2003) Climate-driven increases in global terrestrial net primary production from 1982 to 1999. *Science* 300(5625):1560–1563.
41. Beer C, et al. (2010) Terrestrial gross carbon dioxide uptake: Global distribution and covariation with climate. *Science* 329(5993):834–838.
42. Zhao M, Running SW (2010) Drought-induced reduction in global terrestrial net primary production from 2000 through 2009. *Science* 329(5994):940–943.
43. Jung M, et al. (2011) Global patterns of land-atmosphere fluxes of carbon dioxide, latent heat, and sensible heat derived from eddy covariance, satellite, and meteorological observations. *J Geophys Res* 116(G3), 10.1029/2010JG001566.
44. Keeling CD, Piper SC (2001) Exchanges of atmospheric CO_2 and $^{13}CO_2$ with the terrestrial biosphere and oceans from 1978 to 2000: IV. Critical overview. *SIO Ref Ser* 01-09:1–23.
45. Meir P, Metcalfe DB, Costa ACL, Fisher RA (2008) The fate of assimilated carbon during drought: Impacts on respiration in Amazon rainforests. *Philos Trans R Soc Lond B Biol Sci* 363(1498):1849–1855.
46. Clark DA, Piper SC, Keeling CD, Clark DB (2003) Tropical rain forest tree growth and atmospheric carbon dynamics linked to interannual temperature variation during 1984-2000. *Proc Natl Acad Sci USA* 100(10):5852–5857.
47. Davidson EA, Janssens IA (2006) Temperature sensitivity of soil carbon decomposition and feedbacks to climate change. *Nature* 440(7081):165–173.
48. Rammig A, et al. (2010) Estimating the risk of Amazonian forest dieback. *New Phytol* 187(3):694–706.
49. Cox PM, et al. (2013) Sensitivity of tropical carbon to climate change constrained by carbon dioxide variability. *Nature* 494(7437):341–344.
50. Phillips OL, et al. (2009) Drought sensitivity of the Amazon rainforest. *Science* 323(5919):1344–1347.
51. Lewis SL, Brando PM, Phillips OL, van der Heijden GMF, Nepstad D (2011) The 2010 Amazon drought. *Science* 331(6017):554.
52. Friedlingstein P, et al. (2010) Update on CO_2 emissions. *Nat Geosci* 3(12):811–812.
53. Jones CD, Cox PM (2001) Modeling the volcanic signal in the atmospheric CO_2 record. *Global Biogeochem Cycles* 15(2):453–465.
54. Gu L, et al. (2003) Response of a deciduous forest to the Mount Pinatubo eruption: enhanced photosynthesis. *Science* 299(5615):2035–2038.
55. Mercado LM, et al. (2009) Impact of changes in diffuse radiation on the global land carbon sink. *Nature* 458(7241):1014–1017.
56. Angert A, Biraud S, Bonfils C, Buermann W, Fung IY (2004) CO_2 seasonality indicates origins of post-Pinatubo sink. *Geophys Res Lett* 31(11), 10.1029/2004GL019760.
57. Rossow WB, Schiffer RA (1999) Advances in understanding clouds from ISCCP. *Bull Am Meteorol Soc* 80(11):2261–2287.
58. Wielicki BA, et al. (2002) Evidence for large decadal variability in the tropical mean radiative energy budget. *Science* 295(5556):841–844.
59. Arias PA, Fu R, Hoyos CD, Li W, Zhou L (2010) Changes in cloudiness over the Amazon rainforests during the last two decades: Diagnostic and potential causes. *Clim Dyn* 37(5):1151–1164, 10.1007/s00382-010-0903-2.